Conformational Study of a Bent-Core Liquid Crystal: ^{13}C NMR and DFT Computation Approach

Ronald Y. Dong*,† and Alberto Marini‡,§

Department of Physics and Astronomy, University of British Columbia, Vancouver, BC, V6T 1Z1 Canada, and Dipartimento di Chimica e Chimica Industriale, via Risorgimento 35, Università di Pisa, Italy

Received: May 12, 2009; Revised Manuscript Received: August 6, 2009

A detailed conformational study is carried out by means of density functional theory (DFT) on a bent-core mesogen (A131) in order to shed light on its uniaxial−biaxial nematic phase transition. The most probable conformational states for this V-shaped core are found, from the potential energy surface (PES) of a five-ring model of A131, to fall into two distinct structural groups, namely, the banana-shaped and the hockey-stick-shaped forms. The chemical shielding tensors (CSTs) of the aromatic carbons, for the four prevalent conformers, have been calculated using the GIAO-DFT approach. The derived CSTs are found to compare well with the chemical shift anisotropy (CSA) tensors measured by the 2D-NMR SUPER technique. The CSA tensors are then used to aid the assignment of the aromatic carbon peaks, and the observed ^{13}C chemical shifts from its nematic phases are revisited to provide new structural and local orientational order parameters. In light of the conformational states found from the in vacuo DFT calculations, the "average" configuration shapes of the A131 molecule are found to be different in the nematic phases based on their new local order parameters *S* and *D* of the aromatic rings.

1. Introduction

The biaxial nematic phase has long been sought for in thermotropic liquid crystals (LCs) since its prediction by Freiser in 1970[1] and the experimental observation of a uniaxial to biaxial nematic phase transition in a lyotropic ternary system by Yu and Saupe in 1980.[2] Various attempts to search for this phase in new LC materials composed of calamitic molecules with increasingly anisometric character have not led to too much success.[3] However, bent-core LCs have recently been found to show great promise in rendering biaxial nematic (N_b) phases,[4−6] though more often these new V-shaped molecules give the traditional uniaxial (N_u) phase[7−10] and/or the so-called banana phases. The identification of phase biaxiality in nematogens is by no means trivial and still is a matter of debate. Among many different experimental techniques, deuterium nuclear magnetic resonance (NMR) has been successfully used in quantifying the nematic phase biaxiality in previous works.[2−4] In 2005, several other bent-core LCs were found, based mainly on X-ray studies, to exhibit the N_b phase.[11] The N_u−N_b phase transition is reported at 422 K in a particular V-shaped molecule, 2-methyl-3-[4-(4-octyl-benzoyloxy)-benzylidene]-amino-benzoic acid 4-(4-dodecyl-phenylazo)-phenyl ester (A131), whose molecular structure is shown in Figure 1a. As seen in the figure, A131 is asymmetric not only in the five-ring bent-core region but also contains two lateral alkyl chains of different lengths. The same sample was later studied by ^{13}C solid state NMR techniques,[12] and the preliminary results are consistent with the existence of the N_u−N_b transition upon cooling down from the clearing point. The bend angle Θ in the bent core was also estimated to be 133° in this report. The bend angle is the angle subtended by the two lateral wings next to the central ring and is one of the important structure parameters. It seems to dictate the occurrence of a N_u−N_b transition, and a Θ value of 110° has been predicted to most favor such a phase transition in phase diagrams of bent-core LCs.[3,13]

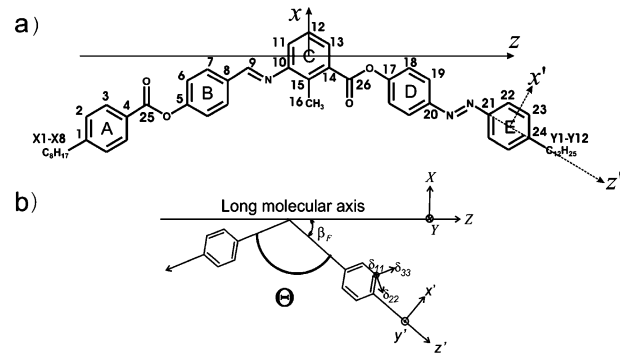

Figure 1. (a) Molecular structure of A131 with carbon site labels. (b) Schematic of a CSA (δ_{11}, δ_{22}, δ_{33}) principal axis frame (PAS), a fragment (x', y', z'), and a molecular frame (x, y, z) fixed on the molecule. Θ is the bend angle of A131, defined as the angle between the axes of the two lateral arms of the bent-core structure.

Detailed density functional theory (DFT) calculations were carrried out to shed light on molecular conformations in the bent core of A131 by searching its conformation energy landscapes and to calculate carbon shielding tensors for all of the carbon atoms in its aromatic core region. This study is particularly relevant, as the existence of the N_u−N_b transition in A131 has recently been questioned[14] based on the electro-optic technique using fairly thin sample cells. This has casted doubt on the X-ray findings[11] and the ^{13}C chemical shift data[12] in the two nematic phases of a bulk sample. Hence, a more careful analysis of the ^{13}C data is in order within the context of our DFT approach. The combined DFT and ^{13}C chemical shift analyses are reported here to give additional insights on the local order parameters, in particular near the N_u−N_b phase transition,

† University of British Columbia.
‡ Università di Pisa.
§ c/o Scuola Normale Superiore, Piazza dei Cavalieri 7, 56126 Pisa, Italy.

10.1021/jp904405n CCC: $40.75
Published on Web 09/29/2009

and to illuminate possible molecular structures adopted by the molecular core in the nematic phase(s) of A131.

2. Theory

To facilitate our discussion, a brief description of the pertinent DFT methods and NMR chemical shifts in mesophases is given, as details can be found in the literature. The direct implementation of the gauge invariant atomic orbitals (GIAO) and the continuous set of gauge transformations (CSGT) methods for calculating nuclear magnetic shielding tensors at both the levels of Hartree−Fock (HF) and DFT has been presented and discussed in detail in ref 15. The GIAO (in Gaussian 03)[16] was first introduced by Ditchfield within the coupled Hartree−Fock scheme.[17] The components σ_{ij} of the nuclear shielding tensor (CST) of a carbon nucleus are related to corresponding ones δ_{ij} of the measured carbon chemical shift anisotropy (CSA) tensor according to the following relation:

$$\sigma_{ij} = K_{ij}\sigma_{\mathrm{ref}} - \delta_{ij} \tag{1}$$

where the offset value, σ_{ref}, corresponds to the isotropic shielding of a reference compound and K_{ij} is the Kronecker delta. The isotropic shielding of the reference compound is either estimated from a gas-phase measurement or assumed from calculations (see below). In order to compare the calculated CSA data with those reported in the literature, we have decided to denote the principal elements of the symmetric part of the chemical shift tensor by $\delta_{33} \geq \delta_{22} \geq \delta_{11}$ (this convention states that δ_{33} corresponds to the direction of the least shielded, σ_{33}, with the highest frequency or highest shift).

The observed ^{13}C $\langle\delta\rangle$ for a molecule with cylindrical symmetry in uniaxial mesophases (N_u and SmA phase) is given by[18]

$$\langle\delta\rangle = \delta_{\mathrm{iso}} + \left(\sqrt{\frac{2}{3}}P_2(\cos\beta_{\mathrm{F}})R'_{2,0} + (\sin^2\beta_{\mathrm{F}})R'_{2,2}\right)S - \frac{2}{3}\left(\sqrt{\frac{3}{8}}(\sin^2\beta_{\mathrm{F}})R'_{2,0} + \frac{1}{2}(1+\cos^2\beta_{\mathrm{F}})R'_{2,2}\right)D \tag{2}$$

where β_{F} is the angle between the fragmental z' axis and the long molecular (z) axis (see Figure 1b) and S ($=S_{zz}$) and D ($=S_{xx} - S_{yy}$) are the nematic order parameter and the (molecular) biaxial order parameter, respectively. $R'_{2,0}$ and $R'_{2,2}$ are written in terms of δ_{ii} and the β angle between the δ_{33} direction and z' axis:

$$R'_{2,0} = \sqrt{\frac{2}{3}}\left[P_2(\cos\beta)(\delta_{33} - \delta_{22}) + \frac{1}{2}(\delta_{22} - \delta_{11})\right]$$
$$R'_{2,\pm2} = \frac{1}{2}[(\sin^2\beta)\delta_{33} + (\cos^2\beta)\delta_{22} - \delta_{11}] \tag{3}$$

The orientation of the CSA tensor in the fragmental (x', y', z') frame requires only the Euler angle β due to uniaxial symmetry (ring flips) of the ring fragment. When referring S and D to the segmental frame, the above equation reduces to (i.e., set $\beta_{\mathrm{F}} = 0$)

$$\langle\delta\rangle = \delta_{\mathrm{iso}} + \frac{2}{3}S'\left[P_2(\cos\beta)(\delta_{33} - \delta_{22}) + \frac{1}{2}(\delta_{22} - \delta_{11})\right] + \frac{1}{3}D'[\delta_{11} - \delta_{22}\cos^2\beta - \delta_{33}\sin^2\beta] \tag{4}$$

The local (fragment) order parameters S' and D' for the lateral phenyl rings of A131 can be derived by fitting the observed ^{13}C chemical shifts from each fragment using eq 4. In the following, the superscripts on the local ordering S' and D' will be omitted for simplicity, with the understanding that they refer to local ordering of each aromatic fragment. It must be pointed out that phase biaxiality is undetectable[18] for aligned samples of $\Delta\chi > 0$ as in the case of A131. In fact, in order to establish the phase symmetry by NMR, it would be necessary to prepare a monodomain sample of the nematic and then change its orientation with respect to the magnetic field. In practice, this can be difficult because one of the directors will always be aligned by the magnetic field of the spectrometer. One should be able to manipulate the orientation of the director by either (i) applying a competing electric field or (ii) spinning the sample about an axis orthogonal to the magnetic field.[3]

Now, the observed chemical shifts for a rigid fragment like the central ring of A131 need some attention. Since the central ring cannot flip or rotate like the lateral phenyl rings, it has a reduced (C_s) symmetry; hence, the Saupe order matrix in the chosen molecular (x, y, z) frame (see Figure 1a) is not diagonal. In other words, there are three nonzero order parameters S_{zz}, $S_{xx} - S_{yy}$, and S_{xz} (S_{xy} and S_{yz} vanish by symmetry). The last order parameter, however, is usually vanishingly small. Even so, this local order tensor (in the (x, y, z) frame) can be fully determined from the five ^{13}C $\langle\delta\rangle$'s obtained for the central ring of A131 using the following equation:

$$\langle\delta\rangle = \delta_{\mathrm{iso}} + \frac{2}{3}\left[\Delta\delta S_{zz} + \frac{1}{2}(\delta_{xx} - \delta_{yy})(S_{xx} - S_{yy}) + 2\delta_{xz}S_{xz}\right] \tag{5}$$

where $\Delta\delta$, the anisotropy of δ with respect to the chosen z axis, is given by

$$\Delta\delta = \delta_{zz} - \frac{1}{2}[\delta_{xx} + \delta_{yy}] \tag{6}$$

and the δ tensor of each carbon can be related to its PAS values by using

$$\delta_{ij} = \sum_{\eta}\cos\theta_{\eta i}\cos\theta_{\eta j}\delta_{\eta\eta} \tag{7}$$

where $\theta_{\eta i}$ is the angle between the PAS η axis and the molecular i axis. It is emphasized that the use of ^{13}C chemical shifts to determine molecular or local order in LC requires the precise knowledge of CSA tenors and their PAS orientations, which can be quite straightforwardly obtained by DFT calculations.

3. Experimental and Computational Details

3.1. Experimental Details. The A131 sample was that used in ref 11. Its transition temperatures (K) are as follows: I (449.5) N_u (422) N_b (391.5) SmC (377.3) SmX (366.4) SmY (355.8) Cr. All of the information concerning the ^{13}C NMR solution and solid state measurements have been detailed and discussed elsewhere.[12] In particular, the principal chemical shift tensor components of each chemically distinguishable ^{13}C in A131 have been extracted from the simulations of the corresponding chemical shift anisotropy (CSA) powder patterns measured by the 2D SUPER technique.[19] The SUPER pulse sequence exploits suitably rotation-synchronized radiofrequency pulses for produc-

ing static powder patterns in the first dimension of the 2D MAS spectra. Due to the nature of a SUPER ("recoupling-type") experiment, the observed CSA powder patterns in f_1 dimension and isotropic carbon-13 chemical shifts in f_2 dimension require proper scaling.[19]

3.2. Computational Details. In this work, all of the DFT calculations have been performed using the Gaussian 03 program,[16] where all of the molecular models were built by means of GaussView 3.0. To shed further light on the experimental NMR work of A131 mesogen,[12] DFT calculations have been performed to obtain the most populated conformational states within its five-ring molecular core. From the variety of theories available to compute CSTs, we have decided to adopt the GIAO[17] for its numerous advantages.[20] Hence, the CST is calculated for all aromatic carbons using in vacuo GIAO-DFT on each of the four prelevant conformers, found in the calculated potential energy surface (PES), and compared with the corresponding experimental values, measured by the 2D SUPER sequence.

Due to the fact that the calculated shielding tensors are very sensitive to the size of the basis set and to the geometry employed, it has been decided to retain the polarized 6-31+G(d) basis set throughout our different geometry optimization at the B3LYP[21] level of theory. Geometries obtained in this way are at least as good and in several cases (such as phenyl-benzoate) better than those obtained at the Möller Plesset theory MP2/6-31+G(d) level, which shows greater sensitivity on the basis set.[22]

In last decades, DFT (with a suitable choice of both functional and basis sets) has succeeded in predicting various molecular properties for systems in the ground state at the equilibrium geometry. This approach, which has a computational cost of the same order as the HF method (considerably less than traditional correlation techniques), often gives a quality of calculations comparable to or even better than those of MP2.[23] In contrast to the HF based methods, it is impossible to grade these functionals at the theory level. The modified Perdew−Wang[24] exchange-correlation functional, called MPW1PW91,[25] is particularly accurate in predicting the chemical shielding property, and is therefore used here for the chemical shielding prediction. Most calculations of the CSTs have been performed using the 6-311+G(d,p) (a larger basis set), as this seems to be the best compromise between accuracy and CPU time-intensive basis set.

Finally, a suitable scale for referencing is required to relate the carbon chemical shielding values (σ scale) and NMR chemical shifts (δ shift scale), which are referenced to some standard. This can be built by computing the chemical shielding σ^{ref} of the reference and then using eq 1. In particular, the CSA tensors can be obtained by referencing the absolute shielding tensors obtained by DFT to the absolute shielding of TMS (185.97 ppm), which is calculated at the same level of theory as for the A131 conformer models. It is noticed that the value of δ_{iso} for TMS obtained by GIAO-DFT calculations is very close to 185.4 ppm, obtained after correction of vibrational averaging, bulk susceptibility, temperature, and relating to a secondary standard.[26] This result confirms the appropriateness of the basis set and functional used in our GIAO-DFT calculations. Indeed, the method adopted in this work has been previously tested, and found to be generally satisfactory for ^{13}C NMR shielding calculations of several different relatively large size organic compounds.[27,28] In particular, the combined computational and solid state NMR (ss-NMR) approach followed in this work has been successfully applied to study magnetic and orientational order properties of a ferroelectric liquid crystal, namely, the ZLL 7/*.[29]

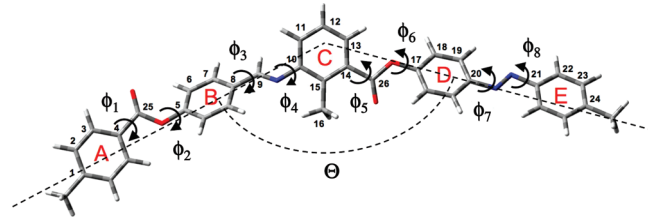

Figure 2. Molecular structure of an **ABCDE** five-ring **5R** model of A131 mesogen.

4. Results and Discussion

4.1. Conformational Analysis. A complete and detailed discussion about the conformational analysis of the A131 molecule has been reported in ref 30; here, we will only give the main important results. In order to accurately study complex systems like A131, its complete structure has been reduced by substituting the long aliphatic chains with methyl units, namely, the 2-methyl-3-[4-(4-methyl-benzoyloxy)-benzylidene]-amino-benzoic acid 4-(4-methyl-phenylazo)-phenyl ester (**ABCDE** model), as shown in Figure 2. This is justified by preliminary tests on a full A131 molecule which have shown that the torsional energies are almost independent of the length of the aliphatic chains. As far as the conformational analysis of the core is concerned, the five-ring (**5R**) approximation is valid if the torsional barriers of the aromatic core rings are not influenced by the aliphatic chain length. This assumption is especially true when investigating local properties such as chemical shielding interaction, because it is closely linked to the environment near the nucleus.[31] In this way, it is possible to investigate quite large molecules with an accurate description of their electronic structures offered by a high level quantum mechanical (QM) approach.

ABC, BCD, and CDE (3R) Models. Even when the **5R** model is adopted to make computations tractable, PES is surveyed initially using three-ring (**3R** model) fragments (i.e., **ABC**, **BCD**, **CDE**). Specifically, the dihedral angles $C_{25}-O-C_5-C_6$ (ϕ_2) and $C_9-N-C_{10}-C_{11}$ (ϕ_4) were scanned in **ABC**, the $C_9-N-C_{10}-C_{11}$ (ϕ_4) and $C_{13}-C_{14}-C_{26}-O$ (ϕ_5) dihedrals for **BCD**, and the $C_{13}-C_{14}-C_{26}-O$ (ϕ_5) and $C_{19}-C_{20}-N-N$ (ϕ_7) dihedrals for **CDE**. Relevant information on torsional barriers and conformational states in each **3R** model were obtained. The PES(**BCD**) shows the highest rotational barriers found among the **3R** models investigated in this work. In particular, it is noticed that the conformations of the **BCD** model determine the orientations of the lateral wings and the bend angle of the entire molecule, because the ϕ_4 and ϕ_5 dihedrals are expected to play a major role in determining the prevalent conformational states in a A131 molecule.

For computational and molecular complexity reasons, it has been decided to select the dihedrals which can reasonably influence the conformations of the A131 molecule, once given a reliable thermal energy at the disposal of the mesogen. Several conformational studies on V-shaped molecules have, therefore, been considered in order to choose the proper angles and to obtain reliable results.[22,32−38]

ABCDE (5R) Model. Four basins of attraction determined in the PES(**BCD**) and labeled by $\Omega(\mathbf{\Gamma}_i)$ for the $\mathbf{\Gamma}_i$ conformers have been surveyed in the **ABCDE** (**5R**) model. Reliable conformers of the **5R** model have been built up in the $\Omega(\mathbf{\Gamma}_i)$ basins by exploiting all of the information gained in the

TABLE 1: Structural Parameters: Dihedral and Bend Angles (in Degrees), Relative Energies (in kcal/mol), and Populations (in %) Evaluated by Boltzmann Distribution at $T = 300$ K, for Γ_i Conformers of the ABCDE Five-Ring Model

conformation	ϕ_2 (deg)	ϕ_4 (deg)	ϕ_5 (deg)	ϕ_7 (deg)	ϑ (deg)	ΔE (kcal/mol)	P (%)
Γ_1	43	44	−165	0	143	0.000	28.50
Γ_2	42	45	−18	0	115	1.076	4.70
Γ_3	42	45	17	0	116	1.413	2.65
Γ_4	43	44	166	0	146	0.417	14.15
Γ_5	43	−44	−166	0	146	0.417	14.15
Γ_6	42	−45	−17	0	116	1.413	2.65
Γ_7	42	−45	18	0	115	1.076	4.70
Γ_8	43	−44	165	0	143	0.000	28.50

conformational study performed on the **3R** models. The four wide basins, characterized by quite low energy regions (less than 2.5 kcal/mol), separated by high energy barriers (from 6 to 12 kcal/mol), contain the eight symmetry related conformers listed in Table 1, whose central core structures are schematically represented in Figure 3.

The obtained Γ_i conformers were subsequently optimized without constraints in geometry in order to obtain fully relaxed structures for the **5R** model, at the same level of theory used for the **3R** models. These fully relaxed and optimized geometries lead to structural parameters very similar to those found for the minimum-energy conformers of the **BCD** model. This suggests that conformations of the **A** and **E** rings have only small influences on the main conformational states of the central core. Nevertheless, it should be noted that conformations of the **A** and **E** rings will play an important role in determining the average bend angle in the nematic phase(s). The in vacuo energy and population for various dominant (symmetry related to ϕ_4 and ϕ_5) conformers are obtained at 300 K and summarized in Table 1. As far as the ϕ_2 and ϕ_7 dihedrals are concerned, for each Γ_i found, there are at least 8 other (4 principal states for $\phi_2 \times 2$ principal states for ϕ_7) populated conformations, not reported here because of symmetry reasons. The structural parameters found for ϕ_2 and ϕ_7 in the Γ_i conformers are in agreement with those found for the most populated conformers in PES(**ABC**) and PES(**CDE**); in particular, the values of $\phi_2 \approx 45°$ and $\phi_7 = 0°$ represent conformations of the lowest energy for these **3R** models. The final full-optimized conformers Γ_1, Γ_2, Γ_3, and Γ_4 have been adopted to calculate the CSTs at the GIAO-DFT level. It has to be noticed that, in vacuo, the Γ_1 and Γ_4 (as well as the symmetry related Γ_5 and Γ_8) conformers are more predominant compared to the others. The molecular structures of the Γ_1 and Γ_3 conformers, shown in Figure 4, show very distinct shapes with a bend angle of 143 and 116°, respectively.

The corresponding angle has been reported[14] as 134° through MOPAC (molecular orbital package), a quantum chemistry program based on Dewar and Thiel's NDDO (neglect of diatomic differential overlap) approximation. Relatively large errors were noted[39] in primarily organic molecules composed of H, C, N, O, and halogen atoms when using the Austin model 1 (AM1) and the parametric method number 3 (PM3), a reparameterized version of AM1 by Stewart, to evaluate bond lengths and dihedral or valence angles. Moreover, the semiempirical rotational barriers are consistently underestimated when compared with experiment. This may be attributed to a possible inadequacy of the MNDO (modified neglect of diatomic overlap)/AM1/PM3 empirical nuclear repulsion functions for describing transition state structures. In particular, correct molecular structures depend on the proper location of potential wells in the PES, and they are intimately related to the energetics of conformational analyses, as found in this study by means of DFT methods.[40] All this considered, the reason for the difference in the bend angle reported in ref 14 can likely be ascribed to both the semiempirical and single-conformer nature of the AM1 calculations.

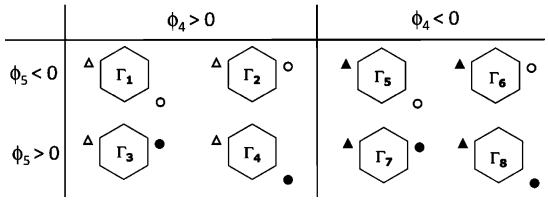

Figure 3. Schematic representation of the eight symmetry related conformations discussed in the text, found for the **ABCDE** model of A131 mesogen. The hexagon stands for the central ring **C**, while the triangles and the circles stand for the iminic (>C═N—) and carboxylic (COO) sp^2 carbons, respectively. Moreover, the open (△ or ○) and filled (▲ or ●) symbols represent above and below positions of the two sp^2 carbons with respect to the aromatic plane of ring **C**, respectively.

4.2. Chemical Shielding Tensor Calculations. The chemical shielding calculations have been performed using fully relaxed structures of the **5R** model. The experimental principal components of the CSA tensors for some carbon sites in A131 were reported.[12] These CSA tensors are now corrected (due to a missing scaling factor of 0.667) and tabulated in Table 2 together with all of the CSA tensors calculated from the in vacuo DFT method for all four Γ_i conformers for direct comparison. Figure 5 shows a comparison among the theoretical chemical shift parameters δ_{ii} (isotropic part and components) for the four relevant conformations Γ_1, Γ_2, Γ_3, and Γ_4 and with the observed NMR chemical shift parameters of A131. The root mean squared deviation (rmsd) evaluated among the Γ_i conformers is ca. ±1 ppm for all of the conformations, showing that there are no significant dependences of the CSA tensors on the different conformational states. As seen in the figure, the differences are mainly observed for the carbons (C11, C12, C13, C14, C15, C17, and C26) located at the central ring **C** and close to it. These findings could be reasonably ascribed to the fact that the chemical shielding interaction is a local property. Nevertheless, when the ϕ_4 and ϕ_5 dihedrals are scanned among the different conformers, the local electron densities of the chemical bonds involved in the rotations indirectly influence the local electron density of the central ring **C**, while almost not those of the lateral rings. It is noticed that the PAS's orientations of all the CST in different conformations are close to those expected from the regular (nominal) geometry, as shown in Table 3.[30] It is obvious that the CST of each ^{13}C involved in the aromatic rings of A131 possesses a principal axis (1 axis, where δ_{11} is placed) oriented perpendicularly to the ring plane, with the two other axes (2 and 3 axis) being in the plane (see Figure 1). Thus, the orientation of each CST is only given by the calculated β angle between the CH (or CC) direction and the principal z' axis of

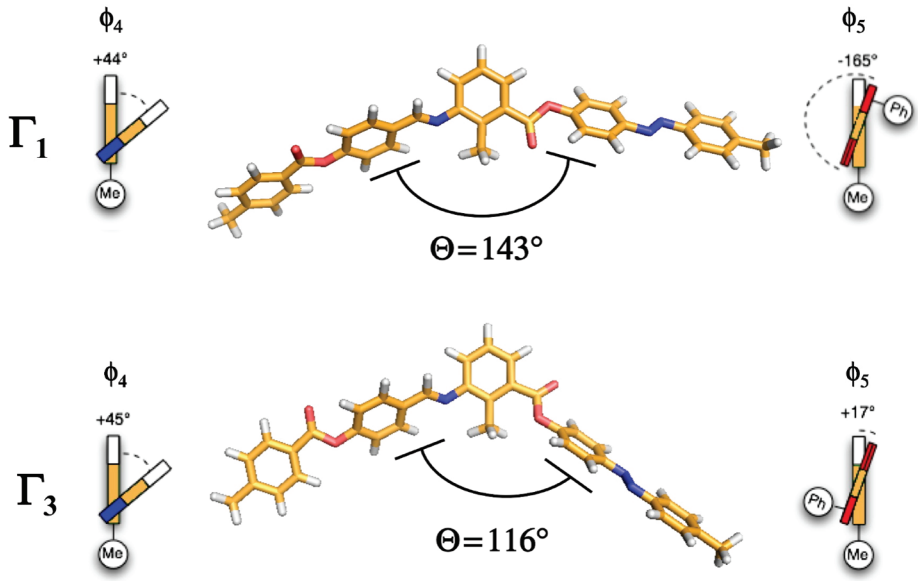

Figure 4. Molecular structures and principal geometrical parameters of the Γ_1 and Γ_3 conformers of the **5R** model for a A131 molecule. Moreover, the lateral side views are shown on the left and right sides of the molecular models.

each fragment. All of the tensor orientations (see Table 3), calculated for the different conformers, show only small variations among themselves and from the "regular" orientation (less than 2°), often assumed and used in solid state NMR experiments. The "regular" orientation (or "regular geometry") assumes that the transformation from the fragment frame (x', y', z') to the PAS frame (δ_{33}, δ_{22}, δ_{11}) involves $\beta = 60$ and 120° for protonated carbons and $\beta = 0°$ for quaternary carbons in a phenyl ring (e.g., ring **A** in Figure 1).

The accuracy of CSA tensors evaluated from 2D SUPER powder patterns of A131[12] is ca. ±3 ppm for each component. In the comparison with the DFT tensors, the root mean squared errors (RMSEs) are about 3, 6, 5, and 4 ppm for δ^{iso}, δ_{11}, δ_{22}, and δ_{33}, respectively, if we exclude carbons C3, C7, C11, C22, and C23,[44] which show fairly noisy SUPER powder patterns.[12] If the comparison is extended to all of the aromatic carbons of A131, the evaluated RMSEs for δ^{iso}, δ_{11}, δ_{22}, and δ_{33} are 3, 10, 14, and 13, respectively, indicating that the experimental CSAs evaluated for carbons C3, C7, C11, C22, and C23 must be taken with some caution (see below) regarding their observed chemical shift anisotropies. Moreover, the relative values of CSA components found for these carbons have the largest deviations from those commonly found in carbons having the same topology and chemical nature.[41] Now the 2D SUPER experiment was carried out in the solid phase, while the DFT calculations were performed in vacuo, which did not account for the effect of molecular packing in the condensed phase. In general, the effect of the medium plays an important role in condensed phases; either structural modifications (*indirect effect*) or, for a given structure, electron density distribution modifications (*direct effect*) can induce significant changes in both the strength (principal components) and orientation of the chemical shielding tensor. Nonetheless, these effects have not been taken into account in this DFT work, because carbon-13 is only slightly affected by these effects. However, this could probably represent an additional source of deviation between the DFT calculated and experimental CSA tensors. All this considered, the values obtained for the principal components of the theoretical δ tensors, in each Γ_i conformer, are in fairly good agreement with those reported in the literature for similar compounds,[29,45] and for generic aromatic systems.[41,46,47]

4.3. Orientational Order Parameters. The observed chemical shifts in the isotropic, N_u, N_b, and SmC phases are reproduced from ref 12 in Figure 6 together with labels for the observed carbons (note that some ^{13}C lines have now been reassigned for correctness). The ^{13}C $\langle\delta\rangle$ in mesophases is related to its isotropic δ_{iso} value by eq 4 for all aromatic carbon sites except for the central ring, for which eq 5 is used instead. To fit the observed $\langle\delta\rangle$'s in the nematic phases, the CSA values listed for A131 in Table 2 can be used. All possible sets of CSA tensors in Table 2 were tested. For the central ring, S_{xz} is found to be vanishingly small (ca. 0.1) for all of the studied temperatures. When the derived Saupe matrix for the central ring is diagonalized to give its S and D, the principal axes of its PAS can also be located. A rotation about the y axis of the (x, y, z) molecular frame is needed for such a diagonalization at each temperature. The original principal z axis only shifts its orientation toward the C12−C26 bond by less than 2° on average. This small change in the z direction is a result of the small S_{xz} value (incidentally, the derived S and D for ring **C** using eq 4 produce in this case the same results).

As the β angles did not deviate much from their nominal values for various CSA tensors, no substantial differences were found when calculating order parameters using "regular" or calculated orientations of the shielding tensors. In LC systems constituted of mainly regular aromatic rings, the use of DFT CST orientation does not have much of an impact on the determination of ordering information, as previously found in ZLL 7/* mesogen.[29] For this reason, we have decided not to further investigate the dependence of ordering on the CST orientations among the different conformers of A131; thus, the following analyses of ^{13}C $\langle\delta\rangle$ are done using the "regular" geometry given in Table 3. We found that the fits to the chemical shifts $\langle\delta\rangle$'s are quite similar for all the cases in which DFT CSA tensors of a particular conformer were used. On the basis of the theory,[3] conformer Γ_1 is supposed to be likely closer to the average shape of an A131 molecule in the N_u phase, while a more bent Γ_3 structure ($\Theta = 116°$) is most likely to be favored in the N_b phase. As an example, the set of CSA tensors for the Γ_3 conformer is chosen here in fitting the chemical shift data. We proceed to fit 22 carbon sites (C1−C8, C10−C15, and C17−C24) using the CSTs of Γ_3 at 13 chosen temperatures in

TABLE 2: Experimental (Corrected 2D SUPER Values from ref 12 due to Missing a Scaling Factor unless Specified Otherwise) and Calculated (GIAO-DFT) Chemical Shift Tensors for Γ_i Conformers of Aromatic Carbon Sites of A131

		δ^{iso}	δ_{33}	δ_{22}	δ_{11}			δ^{iso}	δ_{33}	δ_{22}	δ_{11}			δ^{iso}	δ_{33}	δ_{22}	δ_{11}			δ^{iso}	δ_{33}	δ_{22}	δ_{11}			δ^{iso}	δ_{33}	δ_{22}	δ_{11}
C1	exp	149.4				**C6**	exp	122.4	211.1	145.9	11.7	**C11**	exp	123.6	203.5	145.0	25.1	**C17**	exp	152.3	244.6	149.0	71.0	**C22**	exp	123.6	203.5	145.0	25.1
	Γ_1	145.7	249.4	180.7	7.0		Γ_1	120.5	211	136.9	13.6		Γ_1	121.9	216.1	131.9	17.7		Γ_1	155.1	251.7	140.8	72.7		Γ_1	124.1	219.0	146.3	7.1
	Γ_2	146.2	249.6	181.2	7.9		Γ_2	120.3	210.9	136.7	13.4		Γ_2	121.5	215.4	131.7	17.5		Γ_2	155.4	252.9	139.7	73.7		Γ_2	124.1	219	146.2	7.2
	Γ_3	145.8	249.5	181.0	7.0		Γ_3	121.3	210.5	139.8	13.6		Γ_3	121.3	214.8	131.3	17.7		Γ_3	154.1	251.4	138.1	72.7		Γ_3	124.2	218.8	146.7	7.1
	Γ_4	146.2	249.6	181.2	7.7		Γ_4	121.2	210.7	139.7	13.1		Γ_4	121.4	215.6	130.7	18.0		Γ_4	155.1	251.7	138.5	74.9		Γ_4	124.1	218.8	145.8	7.6
C2	exp	129.1	224.9	137.9	28.5	**C7**	exp	130.5	213.6	170.9	17.2	**C12**	exp	126.5				**C18**	exp	122.4	211.1	145.9	11.7	**C23**	exp	130.5	191.4	159.9	47.4
	Γ_1	128.5	232.7	135.6	17.3		Γ_1	131.1	233.8	150.7	8.8		Γ_1	125	232.9	136.0	6.2		Γ_1	121.3	211.4	138.4	14.0		Γ_1	129.2	232.6	133.9	21.0
	Γ_2	128.6	232.5	135.5	17.8		Γ_2	130.7	232.8	150.6	8.6		Γ_2	125.2	233.3	135.4	7.0		Γ_2	121.8	212.2	137.9	15.3		Γ_2	131.9	235.5	137.5	22.8
	Γ_3	128.3	232.4	135.1	17.3		Γ_3	130.8	233.0	150.5	8.8		Γ_3	125.4	232.8	137.3	6.2		Γ_3	121.1	211.4	137.9	14.0		Γ_3	129.4	233.0	134.1	21.0
	Γ_4	128.4	232.4	135.5	17.5		Γ_4	130.4	232.7	150.4	7.9		Γ_4	125.5	232.6	136.9	7.1		Γ_4	121.4	210.9	138.5	15.0		Γ_4	129.1	232.8	133.7	20.8
C3	exp	130.5	213.6	170.9	17.2	**C8**[a]	exp	129.1	219.3	147.4	14.6	**C13**	exp	129.1	224.9	137.9	28.5	**C19**	exp	124.5	210.2	168.2	−2.7	**C24**	exp	146.3			
	Γ_1	132.7	237.6	154.2	6.2		Γ_1	132.4	219.0	167.7	10.4		Γ_1	131.2	235.4	148.9	9.1		Γ_1	124.5	218.2	148.2	7.0		Γ_1	142.8	247.6	172.3	8.3
	Γ_2	132.0	237.8	153.5	4.8		Γ_2	132.7	219.7	167.4	11.1		Γ_2	132.1	236.1	150.9	9.4		Γ_2	123.3	217.3	147.0	5.6		Γ_2	142.8	247.5	171.6	9.2
	Γ_3	132.2	237.0	153.4	6.2		Γ_3	132.8	219.9	168.1	10.4		Γ_3	130.8	239.3	143.9	9.1		Γ_3	124.4	217.7	148.7	7.0		Γ_3	142.8	247.7	172.4	8.3
	Γ_4	131.5	237.3	153.1	4.2		Γ_4	132.8	219.9	167.4	11.1		Γ_4	129.8	239.6	144.6	5.2		Γ_4	124.4	218.3	147.7	7.1		Γ_4	142.7	247.6	172.2	8.3
C4	exp	126.5	217.8	135.3	30.4	**C9**[b]	exp	159.0	245	163	70	**C14**	exp	134.5	214.6	160.6	30.2	**C20**	exp	151.2	236.4	158.4	57.9	**C25**	exp	164.9	267.8	117.1	106.6
	Γ_1	126.3	216.4	140.6	22.0		Γ_1	158.7	237.5	161.8	76.7		Γ_1	128.7	216.6	140.3	29.1		Γ_1	150.2	232.1	174.7	43.8		Γ_1	163.7	263.3	123.5	104.2
	Γ_2	126.5	217.1	141.0	21.4		Γ_2	159.3	237.9	162.4	77.5		Γ_2	127.4	216.0	138.2	27.9		Γ_2	150.3	232.4	174.2	44.5		Γ_2	164.4	264.3	123.7	105.3
	Γ_3	126.3	216.2	140.7	22.0		Γ_3	158.9	238.2	161.9	76.7		Γ_3	130.4	218.4	143.6	29.1		Γ_3	151.0	232.8	176.3	43.8		Γ_3	163.5	264.8	121.5	104.2
	Γ_4	126.7	217.1	141.0	21.9		Γ_4	159.1	238.1	162.3	77.0		Γ_4	132.1	220.1	143.0	33.3		Γ_4	149.6	232.3	173.2	43.2		Γ_4	164.9	264.4	124.8	105.3
C5	exp	154.1	243.5	150.5	66.5	**C10**[c]	exp	152.3	241	173	35.5	**C15**	exp	134.5				**C21**	exp	151.2	239.4	164.5	43.0	**C26**	exp	164.9	270.0	112.6	102.1
	Γ_1	153.9	249.4	141.5	70.7		Γ_1	153.3	235.7	178.6	45.4		Γ_1	142.4	222.2	190.0	15.0		Γ_1	151.1	234.1	176.9	42.4		Γ_1	164.0	265.5	117.1	109.3
	Γ_2	154.8	250.0	142.6	71.7		Γ_2	153.4	235.7	178.5	45.9		Γ_2	143.3	223.4	190.6	16.1		Γ_2	150.7	234.0	177.1	41.2		Γ_2	163.5	264.4	117.5	108.5
	Γ_3	154.0	249.7	141.6	70.7		Γ_3	152.9	235.6	177.8	45.4		Γ_3	137.7	214.2	184.0	15.0		Γ_3	151.6	234.2	178.2	42.4		Γ_3	167.3	270.7	121.8	109.3
	Γ_4	154.7	250.0	142.5	71.6		Γ_4	153.3	236.4	177.3	46.1		Γ_4	137.6	212.9	184.1	15.8		Γ_4	151.2	233.6	176.5	43.6		Γ_4	166.4	269.3	124.0	105.9

[a] Reference 42. [b] Reference 41. [c] Reference 43.

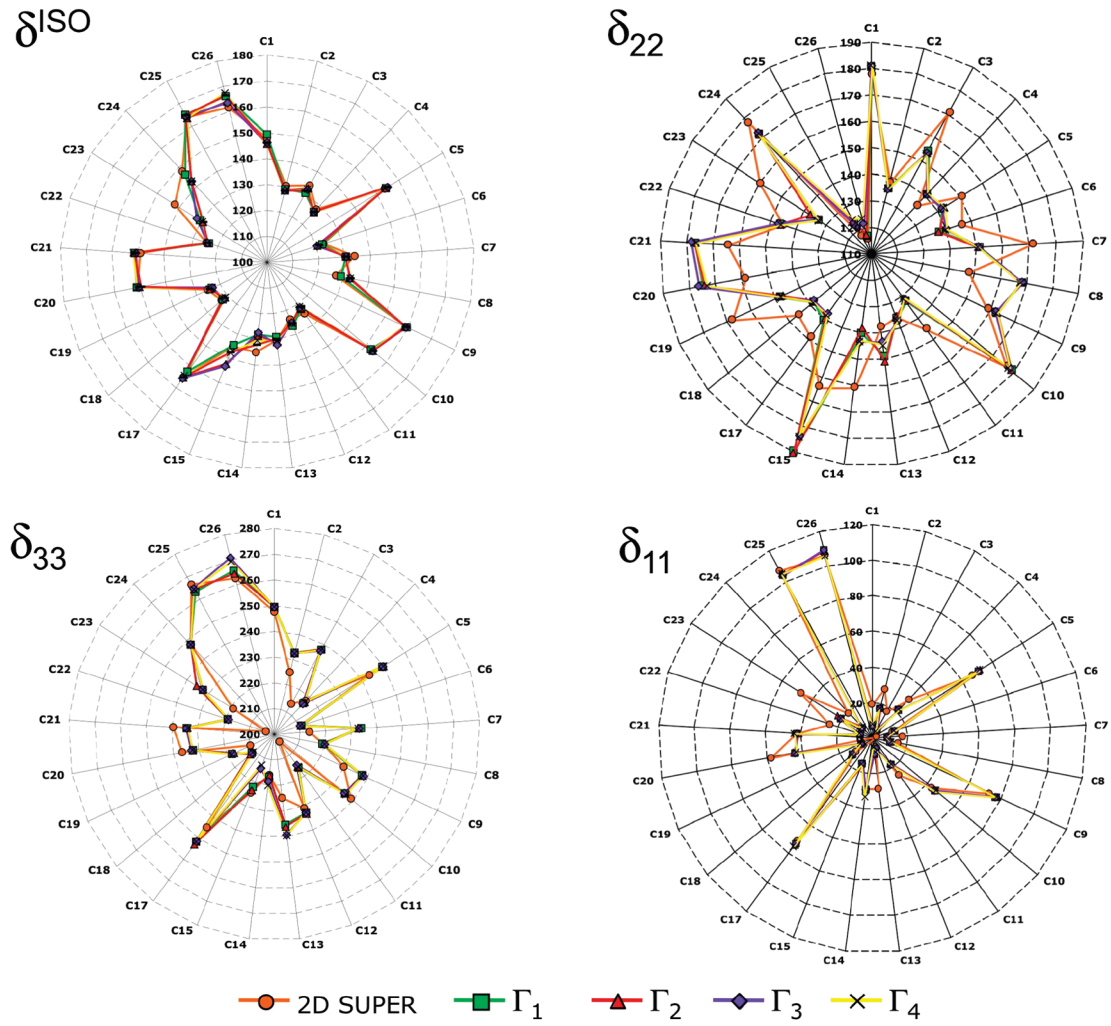

Figure 5. Radial graphs showing the observed dependence of experimental (measured by SUPER (circles) in the solid state at 25 °C) and theoretical (calculated for the four relevant conformations Γ_1 (squares), Γ_2 (trangles), Γ_3 (diamonds), and Γ_4 (crosses) of A131) chemical shift parameters δ_{ii} (isotropic part and components).

TABLE 3: β Angles (Degrees) between the 3 Axis of the Chemical Shift PAS Frame and the *para* Axis of the Relevant Aromatic Fragments (See Figure 1a) among the Different Cases: "Regular" Orientation and DFT Computed Orientation for the Γ_i Conformers of the R5 Model

carbons	reg. geom.	Γ_1	Γ_2	Γ_3	Γ_4	carbons	reg. geom.	Γ_1	Γ_2	Γ_3	Γ_4
C1	180.0	180.0	180.0	180.0	180.0	**C14**	0.0	0.0	0.0	0.0	0.0
C2	120.0	119.6	119.8	119.5	119.3	**C15**	−60.0	−59.8	−59.6	−60.4	−60.7
C3	60.0	59.2	59.4	59.3	59.6	**C17**	180.0	180.0	180.0	180.0	180.0
C4	0.0	0.0	0.0	0.0	0.0	**C18**	120.0	119.8	119.6	120.5	120.3
C5	180.0	180.0	180.0	180.0	180.0	**C19**	60.0	59.6	59.2	60.3	60.4
C6	120.0	120.3	120.8	120.5	120.6	**C20**	0.0	0.0	0.0	0.0	0.0
C7	60.0	60.2	60.4	60.5	60.3	**C21**	180.0	180.0	180.0	180.0	180.0
C8	0.0	0.0	0.0	0.0	0.0	**C22**	120.0	120.2	120.1	119.4	119.8
C9	30.0	34.3	34.7	33.7	33.9	**C23**	60.0	60.4	60.3	60.1	60.6
C10	−120.0	−118.8	−118.7	−120.2	−120.4	**C24**	0.0	0.0	0.0	0.0	0.0
C11	180.0	180.0	180.0	180.0	180.0	**C25**	−30.0	−33.7	−33.4	−34.2	−34.5
C12	120.0	119.3	119.2	119.8	119.5	**C26**	30.0	34.3	34.7	32.6	32.9
C13	60.0	60.3	60.5	59.2	59.4						

the mesophases; the goodness of fits is measured by the sum squared deviation (SSD), yielding a SSD value of 1258 (this corresponds to a rmsd value of about 2.2 ppm on average for each carbon(s) at each temperature). The question is can we do better in the fits, as DFT tensors were derived in vacuo. Thus, we next use all the available CSA tensors obtained experimentally, but noting that when SUPER CSA is unavailable for C1, C12, C15, and C24, the corresponding CSA of Γ_3 was used, while for C8 the CSA of ref 42 was used. The fits are indeed improved somewhat to give a lower SSD of 1136 (which corresponds to a rmsd value of ca. 2.0 ppm).

From these fittings, it is noted that different choices of CSA values do influence the derived local order parameters S and D somewhat. To understand this, it would appear that the in vacuo CSA tensors may not be reflecting the slight perturbation due to the existence of packing or medium effects, even if this effect should be considered very small, as found in ref 29. On the other hand, as pointed out above, some of the CSA tensors

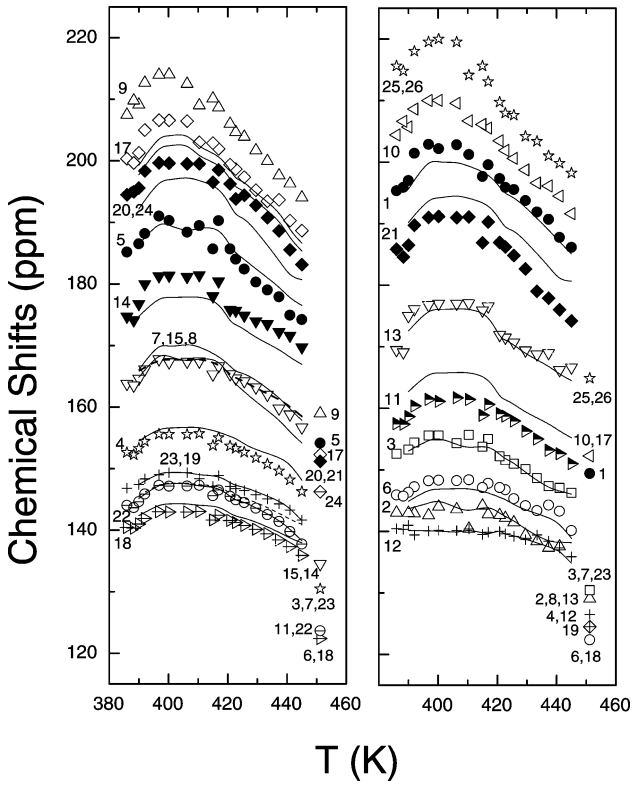

Figure 6. Plots of chemical shifts for the aromatic carbons and linkage carbons of A131 in the isotropic and nematic phases. The carbon labels are those indicated in Figure 1. Theoretical curves (starting from the top, C17, C20, C24, C5, C14, C7, C15 [dashed line], C8, C4, C23, C19 [dashed line], C22, and C18) on the left panel; C1, C21, C13 C11, C3, C6, C2, and C12 on the right panel) denote "best" calculated chemical shifts after a global minimization by varying S and D of each ring (see text).

derived from noisy powder patterns may indeed not be too reliable. To check this possibility, we have replaced those of C7, C19, C22, and C23 (those carbons having fairly noisy SUPER powder patterns) by their corresponding $\mathbf{\Gamma_3}$ CSA values. This corresponds to the best outcome for fitting the same set of ^{13}C $\langle\delta\rangle$'s, as the SSD is further reduced to 1016 (which corresponds to a rmsd of 1.9 ppm), an improvement of ca. 20% when comparing with the SSD using only the $\mathbf{\Gamma_3}$ CSA tensors. The latter calculated $\langle\delta\rangle$'s are also plotted as curves in Figure 6. As seen in this figure, the overall fitting of all the aromatic carbon sites C1−C8, C10−C15, and C17−C24 is quite satisfactory, though systematic deviations do exist for some carbon sites (e.g., C14, C24, and C11 to name a few). The derived "best" S and D parameters are presented in the left panel of Figure 7. Notice that S for all rings increases with decreasing temperature in the N_u phase and tends to level off in the N_b phase. The local S of ring **D** remains the largest among all aromatic rings as noted previously[12] for almost the entire temperature range. Thus, its *para* axis is closest to the "long" molecular axis.

What is more interesting is to examine the behaviors of local biaxial order parameters D in the low temperature N_b phase, particularly for ring **B**. This is because the D parameter reflects the relative degree of ordering of the two minor fragment axes x and y with respect to the major director. Note that ring **B** has the smallest S value among all of the rings and the largest absolute D value, i.e., largest local biaxiality (or S_{yy} tends to zero), that is relatively insensitive to the temperature in the nematic range. The observation for ring **B** can be explained by taking into account two distinct observations: (i) the energy barriers for rotation around the dihedral angles ϕ_2 and ϕ_3 are very low, as found in the DFT calculations, and (ii) the orientation of the *para* axis of ring **B** is highly tilted (it forms an angle of about 60° (see Figure 4), because the rotation of ring **B** around ϕ_4 is restricted, due to the presence of the methyl (C_{16}) unit in ring **C**). Furthermore, D's are negative in the N_b phase for all rings except ring **D**, having a small positive D value (ca. 0.04) but becoming close to zero (tiny biaxiality) in the N_u phase. Physically, this implies the ring **D**'s normal (y axis) to its ring plane is twisted in the opposite sense in the N_b with respect to those of other rings. Furthermore, D of ring **A** appears to go through zero near the (potential) N_u-N_b phase transition and becomes slightly positive in the N_u phase. The observations point to definite changes in the ring plane's orientation of ring **A** and **D** at the N_u-N_b phase transition. Thus, these two rings (**A** and **D**) are likely involved in providing symmetry breaking at the uniaxial to biaxial phase transformation. We will return to this point below in addressing NMR evidence on the bend angle.

As seen in the left panel of Figure 7, S's for all phenyl rings seem to change abruptly across the N_u-N_b phase transition, while their D's move across the transition more smoothly. The N_u-N_b phase transition in A131 may, therefore, be clearly delineated from the trends of S and the observed ^{13}C chemical shifts, especially for carbon sites C5, C13, and C14. To further shed light on the local orientational behaviors of various rings in the A131 bent core, we have decided to also plot $-S_{xx}/S$, a normalized local order (ρ) of the x axis, as a function of temperature in the right panel of Figure 7. Note that ρ has two extreme limits: (i) when S_{yy} tends to zero, ρ has a limiting value of 1 corresponding to maximal ordering of the x axis relative to the major director; (ii) when $D = 0$, then $S_{xx} = S_{yy} = -S/2$ and ρ approaches a limiting value of 0.5. Now, the ρ values of rings **C**, **D**, and **E** are relatively insensitive to temperature over the nematic range (slightly less so for **D**), while rings **A** and **B** show substantial, but opposite, temperature behaviors. Furthermore, the $|S_{yy}|$ is smallest for ring **B**, making S_{xx} a larger negative value, as demonstrated in this figure. Though the reported N_u-N_b transition at around 422 K may not be discerned in this particular plot, it is clear that these two rings (perhaps also ring **D**) are responsible for changing the populations of two (or more) dominant conformers with the temperature. This may seem at first sight to be contrary to the DFT finding that the dihedral angle ϕ_5, the angle that is relevant for rings **C** and **D**, is responsible for the differentiation among the BS and HSS conformations. However, as mentioned above, the (experimental) observed jump up is largest in the C13 and C14 (perhaps also C5) carbons' chemical shift trends at the N_u-N_b phase transition, and remember that the **C**−**D**−**E** fragment, found to be the most "rigid part" (having the highest rotational barriers between **D** and **E**) from DFT, is also the most aligned (**C**−**D**) and ordered part within the aromatic core of A131. This must mean that the local conformational change occurring in the COO group between rings C and D reflects more markedly in the temperature trends in the local order parameter of rings **A** and **B**, as these rings are more orientationally "flexible" and belong to the shorter arm of A131. This local orientation of the **A**−**B** part has made the molecule more biaxial, as indicated in particular by the local biaxial order D of ring **A** (apparent sign change in the two nematic phases).

It would be interesting to see if the above rationale can be reflected through the bend angle. Can this angle be estimated from the local order parameters derived for A131 to collaborate with those from DFT, i.e., the one for the banana-shaped bent-

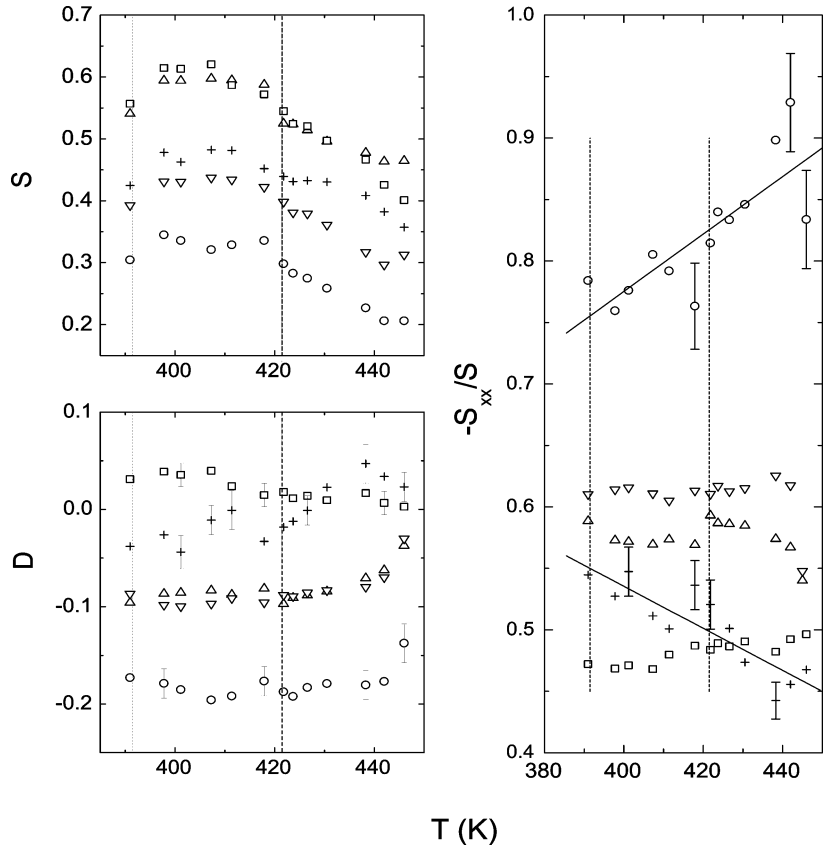

Figure 7. Left: Plots of local order parameters S and biaxial order parameters D of rings **A** (+), **B** (○), **C** (△), **D** (□), and **E** (▽) using SUPER CSA tensors and 8 CSA tensors calculated for the Γ_3 conformer (see text: *case 3*). Right: Plots of "normalized" local order parameters $-S_{xx}/S$ of rings **A** (+), **B** (○), **C** (△), **D** (□), and **E** (▽). Lines are drawn to aid the eyes.

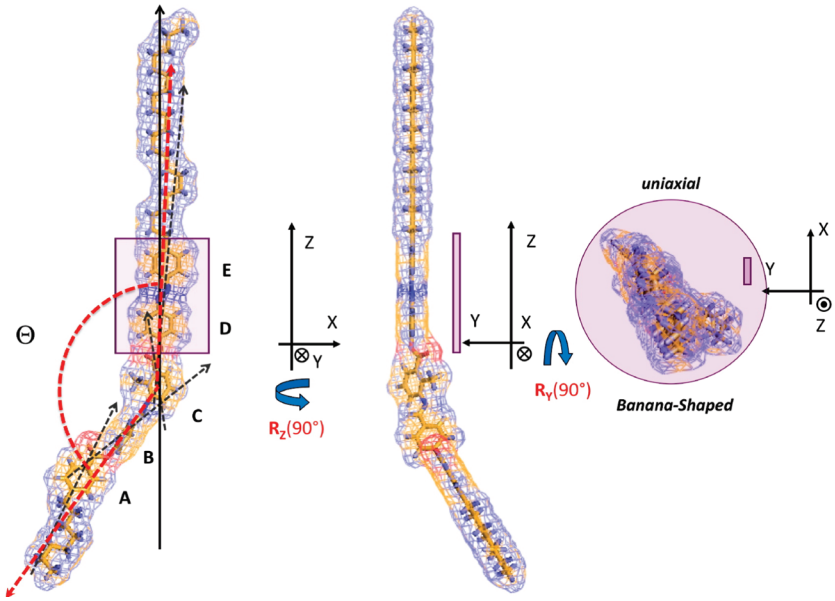

Figure 8. Schematics of the A131 molecule in its uniaxial "banana-shaped" conformation. The cage indicates the surface accessible to the solvent.

core (as observed in the $\Gamma_{1,4}$ conformer), and for the hockey-stick-like conformation (as observed in the $\Gamma_{2,3}$ conformer)? Now the angles between the *para* axes of ring i (i = **A**, **B**, **C**, **E**) and ring **D** (as a reference) can be easily obtained from their S values, from which the Θ can be estimated. It is observed that rings **D** and **E** form a relatively rigid entity due to high rotational barriers (7−8 kcal/mol) for the dihedral rotation of the ϕ_7 and ϕ_8 angles. The bend angle can then be calculated according to the geometry given in Figures 8 and 9 (see also the Supporting Information). From Figure 8, the lower (measured between rings **A** and **E**) and absolute upper (measured between rings **B** and **E**) limits on Θ for BS are ca. 153 and 163°, respectively. Similarly, from Figure 9, the lower and absolute upper limits on Θ for HSS are ca. 111 and 129°, respectively. These estimates for the bend angle may well be a true test of the phase transition in the nematic range of A131,

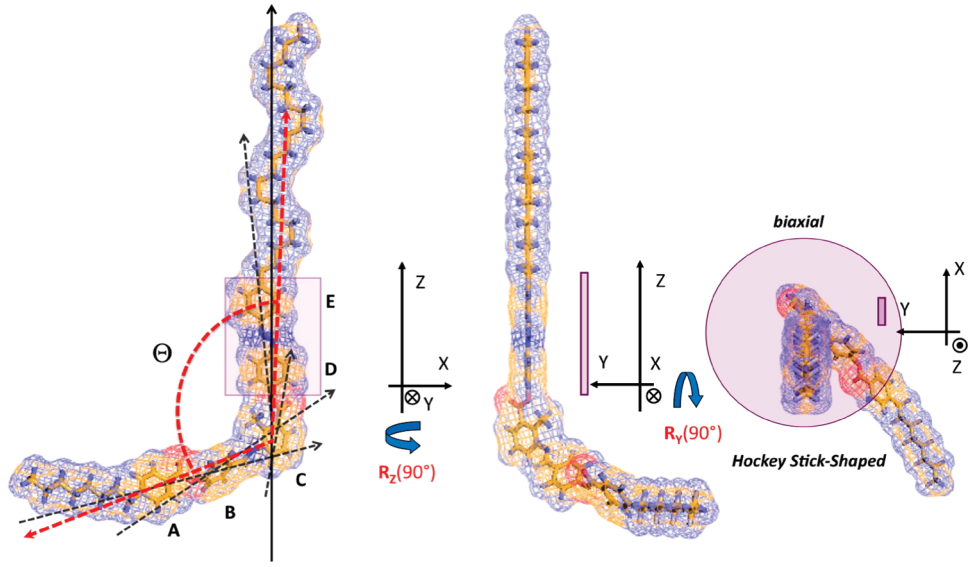

Figure 9. Schematics of the A131 molecule in its nonuniaxial "hockey-stick"-shaped conformation. The cage indicates the surface accessible to the solvent.

as well as support the theoretical prediction of phase diagrams for V-shaped molecules.

In summary, ring **D** on one of the lateral wings (the longer one) is placed in the most rigid part of the A131 molecule (in fact, the rotational barriers around ϕ_5 (4.5 kcal/mol) and ϕ_7 (7−8 kcal/mol) are quite high), and it has been found to have the highest *S* order parameter. The ring plane of ring **D** is seen to twist in the opposite sense from those of the other phenyl rings (giving to the molecule an overall propeller-like shape) upon entering the N_b phase; this is in concert with that of ring **A** at the same transition. It would seem reasonable to expect that the role of flexible end chains cannot be underplayed in the overall configuration of the V-shaped molecule in general, as they must mediate the molecular packing in the underlying SmC phase and/or biaxial nematic phase. Finally, the best SUPER CSA values from the studied molecule should, in principle, be used to gain reliable order parameters. In practice, this may require the augmentation (as done here) by in vacuo DFT calculations for carbon sites with low signal sensitivity and for those having unavoidable spectral crowding. Therefore, we believe the present study has provided a reasonable means to obtain sound local *S* and *D* parameters in mesophases by means of ^{13}C NMR spectroscopy. Indeed, this study has highlighted the reliability and powerfulness of the combined ab initio−solid state NMR spectroscopy approach.

5. Conclusion

The N_u-N_b phase transition in the bent-core A131 mesogen has recently been casted in doubt by an electro-optic study. It was suggested that the observed transition is related to the surface anchoring transition. In this study, it is demonstarted that the normalized local order parameters ρ of rings **A** and **B** have shown quite strong but different temperature behaviors. Note that the conformational average of the molecular shape must depend on the Boltzmann distribution. Our current ss-NMR study can support a phase transition at 422 K and perhaps (less definitive) the biaxial nematic phase. Moreover, the existence of different conformers is clear from both the in vacuo DFT calculations of PES and local order parameters obtained by fitting the ^{13}C chemical shifts $\langle\delta\rangle$'s. The influence of any surface effect on the NMR results can be ruled out, as the studied sample is in the bulk. Indeed, four prevalent conformations (and four symmetry related ones) showing two different bent-core shapes have been revealed. One group of conformers has a bend angle close to 143° and looks more like a "banana"-shaped conformer. The other group has a smaller bend angle of about 116° and resembles more a hockey-stick-shaped structure. There is a strong indication from this study that the DFT bend angles can be rationalized in the two nematic phases on the basis of local *S* and *D* parameters in A131.

When adding the flexible chains to the aromatic bent core and viewing along its "long" axis, the conformers $\mathbf{\Gamma_{1,4}}$ appear like a uniaxial rod (see Figure 8), while those of $\mathbf{\Gamma_{2,3}}$ resemble more a biaxial object (see Figure 9). The schematized molecular shapes are inferred from subtle changes in the orientations of rings **A**, **B**, and **D** in these two nematic phases. In conclusion, it is demonstrated that the question on conformations of the bent-core region in V-shaped molecules can be addressed by DFT calculation of PES in conjunction with the local order parameters obtainable from ^{13}C or ^{2}H ss-NMR spectroscopy. The present study points to the role of rings **A** and **D** (**B**) in influencing the relative populations of at least two dominant bent-core conformers over the entire nematic temperature range. A quantification of relative populations of the uniaxial rod (Figure 8) and biaxial object (Figure 9) would be most interesting and needs further attention. In addition, further studies are necessary to test the postulate on conformational changes within the core region of other V-shaped molecules to search for any potential N_u-N_b transition.

Acknowledgment. R.Y.D. is grateful to Natural Sciences and Engineering Council of Canada for financial support, to Prof. E. E. Burnell for useful discussions, and also to Prof. S. Kumar for introducing the topic of biaxial nematics. A.M. is particularly grateful to Prof. C. A. Veracini for his constant scientific support and Scuola Normale Superiore of Pisa for financial support (Young Researcher 2007 Project Grant).

Supporting Information Available: Tables showing relative energies and populations for $\mathbf{ABC_i}$, $\mathbf{BCD_i}$, and $\mathbf{CDE_i}$ conformers and energy comparisons obtained by AM1, PM3, and DFT and figure showing a plot of the relevant fragmental angles and Cartesian *z* axis systems for the two distinct conformational

states of A131 in its N_u and N_b phases. This material is available free of charge via the Internet at http://pubs.acs.org.

References and Notes

(1) Freiser, M. J. *Phys. Rev. Lett.* **1970**, *24*, 1041.
(2) Yu, L. J.; Saupe, A. *Phys. Rev. Lett.* **1980**, *45*, 1000.
(3) Luckhurst, G. R. *Thin Solid Films* **2001**, *393*, 40.
(4) Madsen, L. A.; Dingemans, T. J.; Nakata, M.; Samulski, E. T. *Phys. Rev. Lett.* **2004**, *92*, 145505.
(5) Acharya, B. R.; Primak, A.; Kumar, S. *Phys. Rev. Lett.* **2004**, *92*, 145506.
(6) Lee, J.-H.; Lim, T.-K.; Kim, W.-T.; Jin, J.-I. *J. Appl. Phys.* **2007**, *101*, 034105.
(7) Niori, T.; Sekine, F.; Watanabe, J.; Furukawa, T.; Takezoe, H. *J. Mater. Chem.* **1996**, *6*, 1231.
(8) Pelzl, G.; Diele, S.; Weissflog, W. *Adv. Mater. (Weinheim, Ger.)* **1999**, *91*, 707.
(9) Dingemans, T. J.; Samulski, E. T. *Liq. Cryst.* **2000**, *27*, 131.
(10) Fodor-Csorba, K.; Vajda, A.; Jakli, A.; Slugovc, C.; Trimmel, G.; Demus, D.; Gacs-Baitz, E.; Holly, S.; Galli, G. *J. Mater. Chem.* **2004**, *14*, 2499.
(11) Prasad, V.; Kang, S.-W.; Suresh, K. A.; Joshi, L.; Wang, Q.; Kumar, S. *J. Am. Chem. Soc.* **2005**, *127*, 17224.
(12) Dong, R. Y.; Kumar, S.; Prasad, V.; Zhang, J. *Chem. Phys. Lett.* **2007**, *448*, 54. This preliminary report unfortunately has missed the scaling factor of 0.667 for the isotropic chemical shifts.
(13) Teixeira, P. I. C.; Masters, A. J.; Mulder, B. M. *Mol. Cryst. Liq. Cryst.* **1998**, *323*, 167.
(14) Van Le, K.; Mathews, M.; Chambers, M.; Harden, J.; Li, Q.; Takezoe, H.; Jakli, A. *Phys. Rev. E* **2009**, *74*, 030701(R).
(15) Cheeseman, J. R.; Trucks, G. W.; Keith, T. A.; Frisch, M. J. *J. Chem. Phys.* **1966**, *104*, 5497.
(16) Frisch, M. J., et al.; *Gaussian 03*, revision B.05; Gaussian, Inc.: Pittsburgh, PA, 2003.
(17) Ditchfield, R. *J. Chem. Phys.* **1972**, *56*, 5688.
(18) Dong, R. Y.; Xu, J.; Zhang, J.; Veracini, C. A. *Phys. Rev. E* **2005**, *72*, 061701.
(19) Liu, S. F.; Mao, J. D.; Schmidt-Rohr, K. *J. Magn. Reson.* **2002**, *155*, 15.
(20) Gauss, J. *J. Chem. Phys.* **1993**, *99*, 3629.
(21) (a) Becke, A. D. *Phys. Rev. A* **1988**, *38*, 3098. (b) Lee, C.; Yang, W.; Parr, R. G. *Phys. Rev. B* **1988**, *37*, 785. (c) Stephens, P. J.; Devlin, F. J.; Chabalowski, C. H.; Frisch, M. *J. Phys. Chem.* **1994**, *98*, 11623.
(22) Wrzalik, R.; Merkel, K.; Kocot, A. *J. Mol. Model.* **2003**, *9*, 248.
(23) Wiberg, K. B. *J. Comput. Chem.* **1999**, *20*, 1299.
(24) Perdew, J. P. In *Electronic Structure of Solids 91*; Ziesche, P., Eschig, H., Eds.; Akademie Verlag: Berlin, 1991; p 11.
(25) (a) Adamo, C.; Barone, V. *J. Chem. Phys.* **1998**, *108*, 664. (b) Lynch, B. J.; Zhao, Y.; Truhlar, D. G. *J. Phys. Chem.* **2003**, *107*, 1384.
(26) Mason, J. *Multinuclear NMR*; Plenum Press: New York, 1987; Chapter *3*.
(27) Catalano, D.; Geppi, M.; Marini, A.; Veracini, C. A.; Urban, S.; Czub, J.; Kuczynski, W.; Dabrowsky, R. *J. Phys. Chem. C* **2007**, *111*, 5286.
(28) Geppi, M.; Marini, A.; Veracini, C. A.; Urban, S.; Czub, J.; Kuczynski, W.; Dabrowsky, R. *J. Phys. Chem. B* **2008**, *112*, 9663.
(29) Dong, R. Y.; Geppi, M.; Marini, A.; Hamplova, V.; Kaspar, M.; Veracini, C. A.; Zhang, J. *J. Phys. Chem. B* **2007**, *111*, 9787.
(30) Marini, A., Prasad, V., Dong, R. Y. In *Nuclear Magnetic Resonance Spectroscopy of Liquid Crystals*; Dong R. Y., Ed.; World Scientific Publishing Co.: Singapore, 2009.
(31) Kaupp, M., Buhl, M., Malkin, V. G. *Calculation of NMR and EPR Parameters*; Wiley VCH: Weinheim, Germany, 2004.
(32) Imase, T.; Kawauchi, S.; Watanabe, J. *J. Mol. Struct.* **2001**, *560*, 275.
(33) Cacelli, I.; Prampolini, G. *Chem. Phys.* **2005**, *314*, 283.
(34) Calucci, L.; Forte, C.; Fodor-Csorba, K.; Mennucci, B.; Pizzanelli, S. *J. Phys. Chem. B* **2007**, *111*, 53.
(35) Wang, L.; Wang, X. *J. Mol. Struct.* **2007**, *806*, 179.
(36) Emsley, J. W.; C Furby, M. I.; De Luca, G. *Liq. Cryst.* **1996**, *21*, 877.
(37) Tsuji, T.; Takeuchi, H.; Egawa, T.; Konaka, S. *J. Am. Chem. Soc.* **2001**, *123*, 6381.
(38) Inoue, K.; Takeuchi, H.; Konaka, S. *J. Phys. Chem. A* **2001**, *105*, 6711.
(39) Dewar, M. J. S.; Jie, C. X.; Yu, J. G. *Tetrahedron* **1993**, *49*, 5003.
(40) Cramer, C. J. *Essentials of Computational Chemistry*, 2nd ed.; J. Wiley & Sons, Ltd.: Chichester, England, 2004.
(41) Duncan, T. M. *Principal Components of Chemical Shielding Tensors: a compilation*, 2nd ed.; The Farragut Press: Madison, WI, 1997.
(42) Zheng, G.; Hu, J.; Zhang, X.; Shen, L.; Ye, C.; Webb, G. A. *J. Mol. Struct.* **1998**, *428*, 283.
(43) Parhami, P.; Fung, B. M. *J. Am. Chem. Soc.* **1985**, *107*, 7304.
(44) These carbons show very noisy 1D powder pattern slices, partially due to the overcrowding of ^{13}C signals (derived from the complexity of the system under study) but mostly due to the small quantity of the available A131 sample.
(45) Nakai, T.; Fujimori, H.; Kuwahara, D.; Miyajima, S. *J. Phys. Chem. B* **1999**, *103*, 417.
(46) Kolbert, A. C.; Griffin, R. G. *Chem. Phys. Lett.* **1990**, *166*, 87.
(47) Hu, J. Z.; Orendt, A. M.; Alderman, D. W.; Pugmire, R. J.; Ye, C.; Grant, D. M. *Solid State Nucl. Magn. Reson.* **1998**, *3*, 181.

JP904405N